

Simultaneous Direct and Indirect Wavefront Sensing Using Multiplexed Programmable Grating Patterns

Biswajit Pathak^a

^aDepartment of Engineering Science, University of Oxford, Parks Road, Oxford OX1 3PJ, UK

ABSTRACT

Direct wavefront sensing is commonly performed by using a popular Shack-Hartmann wavefront sensor. On the other hand, indirect wavefront sensing is performed based on an image quality metric by acquiring a sequence of images in which pre-determined amount of aberrations modes are incorporated. Both the sensing approaches have their advantages and disadvantages depending on specific applications. In the present work, we propose simultaneous realization of both the sensing approaches with broader applications by using a multiplexed programmable binary diffraction grating pattern. We present proof-of-concept simulation results that demonstrate the working of the proposed multiplexed grating array based wavefront sensor (MGAWS) and its flexibility in easy switching between both the sensing approaches to estimate the wavefront accurately.

1. INTRODUCTION

A conventional photo sensitive detector capable of measuring only the intensity or brightness level of a light beam cannot directly measure the wavefront of an incident beam. However, the wavefront can be measured if the detector is allowed to receive a deformed wavefront (by deformed wavefront, we mean the deviation of the wavefront with respect to an ideal or plane wavefront). This deviation causes a change in the focal spot, relative to the focal spot obtained due to a plane wavefront. The change may be in the intensity level of the focal spot, shape of the focal spot, shift in the centroid of the focal spots, etc. All these variations of the focal spot on the detector plane, are directly linked to the deformed wavefront, which can be analyzed further to estimate the incident wavefront. Thus, based on these roundabout approaches where the focal spot is allowed to change differently, the wavefront sensing approaches are broadly classified into zonal wavefront sensing and modal wavefront sensing.¹ The zonal and modal wavefront sensing are also often referred to as direct and indirect wavefront sensing.

In the case of zonal wavefront sensing, an incident wavefront is sampled to express it locally over a finite number of discrete zones or small spatial areas. This type of sensing is performed by one of the popularly used zonal sensors, such as the Shack Hartmann wavefront sensor (SHWS), named after Johannes Franz Hartmann and Roland Shack² (we refer to the device as sensor and to the approach/method as sensing). It is a modified version of the original Hartmann wavefront sensor developed in 1904 by J. Hartmann.^{3,4} The SHWS consists of a two dimensional (2D) array of lenslets (each having same focal length and aperture size) along with a detector placed at the common focal plane of these lenslets. The detector is used to capture the focal spot corresponding to each of the lenslets. A regularly spaced grid of spots are obtained on the focal plane of the lenslets array for a plane incident wavefront. However, introduction of any deformation into the incident wavefront will displace the spots from their original locations (also known as the reference position). The shift of the focal spot centroid positions with respect to the reference positions depends on the information of the local wavefront slopes of the incoming deformed wavefront. These local slope information can be used in an estimation algorithm^{1,5} in order to obtain the phase profile of the incident wavefront. In the case of modal wavefront sensing,^{6,7} the entire incident wavefront information is collected globally in terms of on-axis intensity distribution variation on the focal plane by acquiring a sequence of images. The sequence of images are acquired by deliberately adding and subtracting the same amount of an orthogonal aberration mode (such as Zernike modes) from the incident wavefront (by making two identical copies of the incident wavefront). An image quality metric is defined with parameters such

Further author information: (Send correspondence to B.P.)

B.P.: E-mail: biswajit.pathak@eng.ox.ac.uk

as, image sharpness, maximum intensity, average intensity, etc., which are then used in an optimization process to obtain the aberration modes present in the incident wavefront.

A programmable version of the zonal wavefront sensor is the grating array based wavefront sensor (GAWS) that uses a 2D array of plane binary diffraction gratings and a single focusing lens.^{8,9} This arrangement thus replaces the lenslets array of the SHWS and is implemented using a liquid crystal spatial light modulator (LCSLM), employing a computer generated holography (CGH) technique. If a collimated laser beam is incident on the grating array, it generates $\pm n$ diffracted orders ($n = \pm 1, \pm 3, \pm 5$, etc). Among the various diffracted orders, the +1 order from each grating element is primarily chosen (due to its high intensity) to result in a regular 2D array of spots on the camera plane for an unaberrated incident wavefront. The centroid shifts of the diffraction spots thus can be considered similar to that of the focal spot array of the SHWS. Thus, the GAWS works in a similar principle as that of the SHWS with some added advantages owing to its programmable nature. Similarly, in the programmable version of the modal wavefront sensor,^{10,11} a binary hologram can be created using an LCSLM, employing CGH technique that gives rise to $\pm n$ diffracted orders. As any of the diffracted orders can carry a user defined phase function, the +1 and -1 diffracted orders can be treated as the positive and the negative bias beams, respectively. Moreover, it is also possible to create a duplexed or multiplexed hologram that gives rise to a single pair of +1 orders (or -1 orders) or multiple pairs of +1 orders (or -1 orders), respectively.^{12,13} Both the type of wavefront sensors have their advantages and disadvantages. The modal wavefront sensor is fast and works well in the presence of lower order aberrations or single aberration mode. However, its performance decreases in the presence of large aberrations or with the increase in the number of modes present in the incident wavefront due to modal cross-talk.^{14,15} The zonal wavefront sensor is expected to perform better in this case. In practicality, there will be presence of either single aberration mode or a combination of different aberration modes. Moreover, in many cases there is no prior knowledge about the types of aberration present in the incident wavefront. Thus in such situations, using both the type of sensors simultaneously may be necessary to detect and compensate for these aberrations more accurately.

In the present work, we propose to design a multiplexed grating array based wavefront sensor (MGAWS) that can be used to perform both the zonal and modal wavefront sensing simultaneously by using a multiplexed programmable binary diffraction grating pattern. The transmittance function of the grating pattern is defined to simultaneously generate an array of two dimensional +1 order spots and a pair of +1 order spots. Thus, the proposed sensor can be programmed to function either as a zonal/modal sensor or both, depending on the type of aberrations or applications. We present proof-of-concept simulation results that demonstrate the working of the proposed sensor and its capability to estimate the wavefront accurately.

2. MULTIPLEXED GRATING ARRAY BASED WAVEFRONT SENSOR

The proposed MGAWS is designed by defining a complex transmittance function of the grating pattern. The mathematical algorithm defining the transmittance of the 2D array of binary diffraction grating pattern $g_t(x, y)$, having a pixel resolution of $N_x^g \times N_y^g$ (where $N_x^g = N_y^g$) to generate two sets of n^{th} diffracted orders can be written as

$$g_t(x, y) = \begin{cases} 1 & \text{if } \text{real} \left[e^{i(m_{0x}^i x + m_{0y}^j y)} + e^{i(\phi^M(x, y) + (f_{Nx}^{k1, k2} x + f_{Ny}^{l1, l2} y))} \right] \geq 0 \\ 0 & \text{if } \text{real} \left[e^{i(m_{0x}^i x + m_{0y}^j y)} + e^{i(\phi^M(x, y) + (f_{Nx}^{k1, k2} x + f_{Ny}^{l1, l2} y))} \right] < 0 \end{cases} \quad (1)$$

here (m_{0x}^i, m_{0y}^j) is given as,

$$\begin{aligned} m_{0x}^i & \left|_{i=1}^{i=N} = m_{0x}^1 + (i - 1) \times \Delta m_{0x} \\ m_{0y}^j & \left|_{j=1}^{j=N} = m_{0y}^1 + (j - 1) \times \Delta m_{0y} \end{aligned} \quad (2)$$

where, N is the grating dimension, (m_{0x}^1, m_{0y}^1) is the spatial frequency of the top left grating element (i.e., 1,1) and $(\Delta m_{0x}, \Delta m_{0y})$ are real numbers that apply a uniform increment between the adjacent grating elements along i (row index) and along j (column index). Considering $\Delta m_{0x} = \Delta m_{0y}$, will result in a square array of $\pm n$ diffracted spots (here +1 order is considered due to highest intensity) of dimension $N \times N$ in the focal plane. The formation of the diffracted orders in the focal plane can be explained by performing a Fourier series expansion of the transmittance function of the grating pattern.^{16,17} Each of these orders are diffracted to spatially separated positions as each of them contains a different overall tilt.

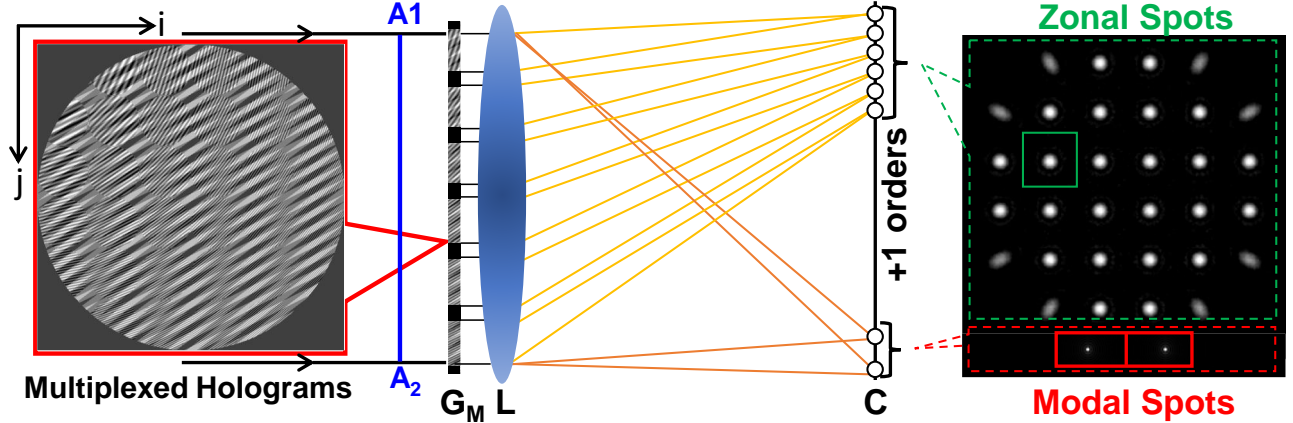


Figure 1. A schematic diagram of the principle of proposed multiplexed hologram based wavefront sensor is illustrated that results in two sets of +1 order spots, namely zonal spots (within green dotted box) and modal spots (within red dotted box).

A duplex hologram is defined with total pixel resolution of $N_x^d \times N_y^d$ (where $N_x^d = N_y^d$) such that $N_x^d = N_x^g \times N$ to generate a pair of +1 orders. The spatial frequencies of the duplex hologram is also defined in a similar way as that for the grating array, where $(f_{Nx}^{k1}, f_{Nx}^{k2})$ and $(f_{Ny}^{l1}, f_{Ny}^{l2})$ denotes the spatial frequencies of the two holograms along both the horizontal and vertical directions, such that $f_{Nx}^{k1} \neq f_{Nx}^{k2}$, $f_{Ny}^{l1} = f_{Ny}^{l2}$ and $f_{Ny}^{l1} > m_{0y}^j|_{j=N}$, in order to place the pair of +1 orders spatially separated with respect to the 2D array of +1 orders, along vertical direction (although any other placement works equally well as long as both the sets of +1 orders are spatially separated). The duplex hologram is updated sequentially by using the phase function $\phi^M(x, y)$ such that each aberration mode is measured at a time. This will result in M number of bias +1 order pairs if M number of total aberration modes are to be measured.

A diagrammatic representation of the principle of multiplexed hologram based wavefront sensor is illustrated in Fig. 1. If a collimated light beam is incident on the 2D multiplexed binary grating pattern, represented by G_M then in the focal plane of the lens L , a regular 2D array of +1 orders (shown within the green dotted box) and another pair of spatially separated +1 orders (shown within the red dotted box) will be generated, corresponding to the plane incident wavefront A_1A_2 . The 2D array of +1 orders will be used to perform the zonal sensing, whereas the other pair of +1 order will be used to perform the modal sensing. Thus, for the purpose of simplicity, we refer to the 2D array of spots as the zonal spots and the pair of +1 order spots as the modal spots.

3. RESULTS AND DISCUSSION

We perform simulations to illustrate the working of the proposed MGAWS that is capable of generating both the zonal and modal spots simultaneously. Numerical simulations were performed in MATLAB software (Matlab version R2015b) to construct the 2D multiplexed binary diffraction grating pattern using Eq. 1 where the duplexed hologram is defined with a pixel resolution of 512×512 and each grating element of the 2D array is defined with a pixel resolution of 85×85 such that it has a grating array dimension of 6×6 . Both the zonal and modal spots were obtained by performing Fourier Transform operations over the 2D multiplexed binary grating pattern. The slope information from the centroid shift measurements (using standard center of mass algorithm) is obtained using the zonal spots by defining detector sub-apertures equivalent to that of the full-width at half maximum (FWHM)

of a spot near the center. Similarly, the average intensity (used as a quality metric parameter) information is obtained by defining another pair of detector sub-apertures equivalent to the FWHM of a modal spot, free of aberration. Using CGH technique, we can make the incident wavefront to be holographically aberrated with a user defined phase function $\Phi(x, y)$ (similar to the one shown in Eq. 1) to represent a beam with classical aberrations expressed as a linear combination of single indexed Zernike polynomials¹⁸ (Z_j), such that $\Phi(x, y) = \sum a_j Z_j(x, y)$ (where a_j represents the root mean square amplitudes of the j^{th} mode in radians). The slope and intensity information are obtained simultaneously to estimate the incident wavefront by using the Southwell algorithm¹ (zonal estimation method) and the parabolic maximization process¹¹ (obtaining a minimum of $2M+1$ value of the quality metric for M number of aberration modes to be measured), respectively.

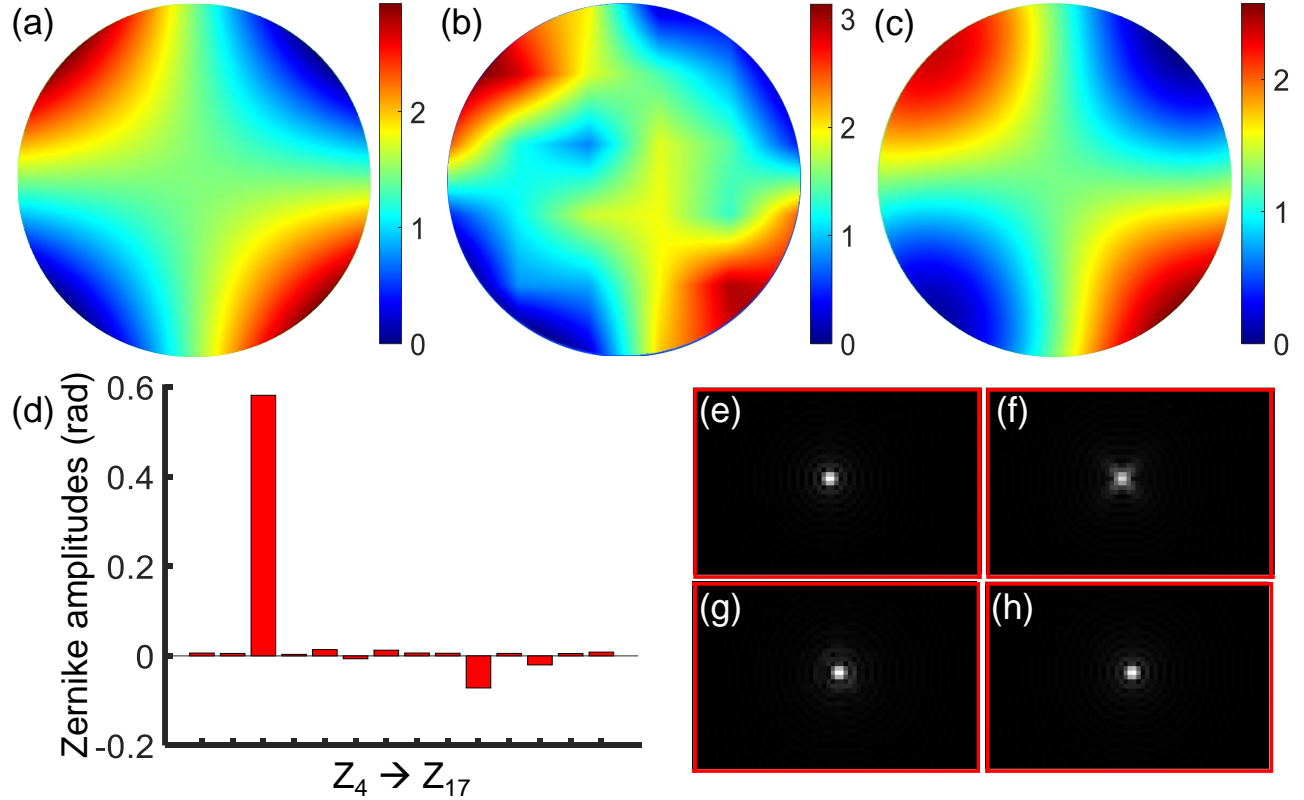


Figure 2. False color images representing the (a) applied phase profile, $\Phi(x, y) = 0.6Z_6$ and the estimated wavefront using the (b) zonal and the (c) modal sensing of the proposed sensor are illustrated. The RMS amplitudes of the Zernike modes detected in the case of modal sensing is shown as bar diagram plot in (d). The focal spot images (e) before addition of $\Phi(x, y)$ and (f) after addition of $\Phi(x, y)$ which is later compensated using the (g) zonal sensing and (h) modal sensing are illustrated. The axis labels appearing in all the images have the unit of radian.

We present simulation results that demonstrate the simultaneous wavefront estimation by zonal and modal sensing using the proposed sensor, in the presence of lower order aberration and a combination of lower and higher order aberrations. Figure 2(a) shows the applied phase profile for $\Phi(x, y) = 0.6Z_6$ and the corresponding estimated wavefront using the zonal and modal sensing are shown in Fig. 2(b) and Fig. 2(c), respectively. The bar diagram plot in Fig. 2(d) represent the RMS amplitudes of the Zernike modes detected in the case of modal sensing (Zernike modes $Z_4 \rightarrow Z_{17}$ were considered). Figure 2(e) and Fig. 2(f) represents the focal spot obtained before and after addition of $\Phi(x, y)$, respectively. Figure 2(g) and Fig. 2(h) represents the focal spot obtained after compensation (using the optical phase conjugation technique) of the aberration (resulting from the applied phase profile) using the zonal and modal sensing, respectively. The value of root mean square (RMS) errors calculated from the difference between applied and estimated phase profiles are found to be 0.4456 radian and 0.2250 radian for the zonal and modal sensing, respectively. We present another set of similar simulation results as shown in Fig. 3, where the applied phase profile is a combination of lower and higher order Zernike modes,

given as $\Phi(x, y) = -0.6Z_5 + 0.8Z_8 + 0.4Z_{11} - 0.5Z_{14}$. The value of RMS errors calculated are found to be 0.9260 radian and 1.3919 radian for zonal and modal sensing, respectively. All the plots in Fig. 2 and Fig. 3 are in radian units.

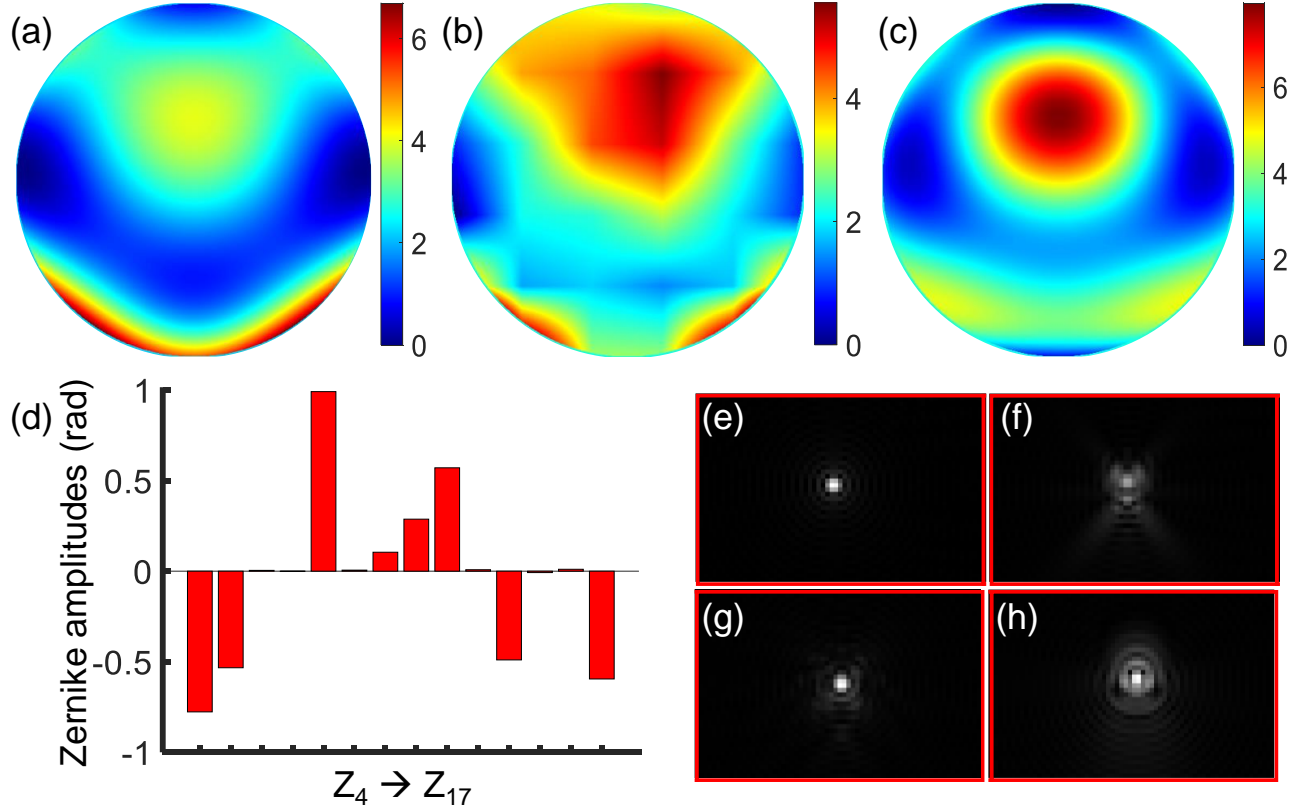


Figure 3. False color images representing the (a) applied phase profile, $\phi(x, y) = -0.6Z_5 + 0.8Z_8 + 0.4Z_{11} - 0.5Z_{14}$ and the estimated wavefront using the (b) zonal and the (c) modal sensing of the proposed sensor are illustrated. The RMS amplitudes of the Zernike modes detected in the case of modal sensing is shown as bar diagram plot in (d). The focal spot images (e) before addition of $\Phi(x, y)$ and (f) after addition of $\Phi(x, y)$ which is later compensated using the (g) zonal sensing and (h) modal sensing are illustrated. The axis labels appearing in all the images have the unit of radian.

From the above results, it is evident that the modal sensing performs better in the case of a single lower order mode present in the applied phase profile (this is also clear from the RMS error values). However, when the applied phase profile contains a combination of different Zernike mode amplitudes, the zonal sensing performs better than the modal sensing due to increase in the modal cross-talk in the latter. This is also clear from the RMS error value and the focal spot image shown in Fig. 3(g) that compensate the aberration (resulting from the applied phase profile) to closely match with the aberration free focal spot (diffraction limited) in comparison to the focal spot image shown in Fig. 3(h). There is a possibility of further improving the aberration compensation, if both the sensing approaches are used consecutively rather than simultaneously. It is to be mentioned that for the purpose of comparison of both the sensing approaches, we have used standard algorithms and quality metric parameters. However, the performance of each of the sensing approaches can be individually improvised, such as by increasing the wavefront sampling frequency or by considering an improved estimation algorithm in the case of zonal sensing, whereas, by using a different quality metric parameter, different fitting algorithm (other than the parabolic fitting) or by acquiring more sequence of images with different bias values, in the case of modal sensing.

4. CONCLUSION

In conclusion, we have proposed a multiplexed grating array based wavefront sensor capable of performing both the zonal and modal wavefront sensing. Exploiting the programmable facility, we define the transmittance function of the sensor to construct an array of multiplexed grating patterns to generate two sets of +1 diffracted orders simultaneously. One set, corresponding to the zonal spots measure the local slope of the incident wavefront to perform the zonal sensing, whereas the other set, corresponding to the modal spots measure average intensity variation to perform the modal sensing. Through simulations we have demonstrated that the proposed sensor can perform both the sensing simultaneously. Further, we have also showed that the proposed sensor can compensate for the presence of either a single mode aberration or a combination of aberrations, with the ease of switching between the sensing approaches as per requirement.

ACKNOWLEDGMENTS

Author would like to acknowledge the facilities provided by University of Oxford to carry out the simulation work presented here.

REFERENCES

- [1] W. H. Southwell, "Wave-front estimation from wave-front slope measurements," *J. Opt. Soc. Am.* **70**, 998–1006 (1980).
- [2] R. V. Shack, "Production and use of a lecticular hartmann screen," *J. Opt. Soc. Am.* **61**, 656–661 (1971).
- [3] J. Hartmann, "Objektuvuntersuchungen," *Zt. Instrumentenk* **24**, (1904).
- [4] B. C. Platt and R. Shack, "History and principles of Shack-Hartmann wavefront sensing," *J. Refract. Surg.* **17**, S573–S577 (2001).
- [5] B. Pathak and B. R. Boruah, "Improved wavefront reconstruction algorithm for shack-hartmann type wavefront sensors," *J. Opt.* **16**, 055403 (2014).
- [6] M. A. A. Neil, M. J. Booth and T. Wilson, "New modal wave-front sensor: a theoretical analysis," *J. Opt. Soc. Am. A* **17**, 1098–1107 (2000).
- [7] M. J. Booth, "Adaptive optics in microscopy," *Philos. Trans. R. Soc. A* **365**, 2829–2843 (2007).
- [8] B. R. Boruah, "Zonal wavefront sensing using an array of gratings," *Opt. Lett.* **35**, 202–204 (2010).
- [9] B. Pathak, "Development of a zonal wavefront sensor with enhanced performance using a reconfigurable array of binary diffraction gratings," PhD Thesis, IIT Guwahati Chapter **3**, (2017).
- [10] M. A. A. Neil, M. J. Booth and T. Wilson, "Closed-loop aberration correction by use of a modal Zernike wave-front sensor," *Opt. Lett.* **25**, 1083–1085 (2000).
- [11] M. J. Booth, "Direct measurement of Zernike aberration modes with a modal wavefront sensor," *Proc. SPIE* **5162**, 79–90 (2003).
- [12] F. Ghebremichael, G. P. Andersen, and K. S. Gurley, "Holography-based wavefront sensing," *Appl. Opt.* **47**, A62–A69 (2008).
- [13] G. P. Andersen, L. C. Dussan, F. Ghebremichael, and K. Chen, "Holographic wavefront sensor," *Opt. Eng.* **48**, 085801 (2009).
- [14] S. K. Mishra, R. Bhatt, D. Mohan, A. K. Gupta, and A. Sharma, "Differential modal Zernike wavefront sensor employing a computer-generated hologram: a proposal," *Appl. Opt.* **48**, 6458–6465 (2009).
- [15] F. Loosen, J. Stehr, L. Alber, I. Harder, and N. Lindlein, "A holography-based modal wavefront sensor for the precise positioning of a light emitter using a high-resolution computer-generated hologram," *IEEE Photonics J.* **10**, 1–11 (2018).
- [16] M. A. A. Neil, M. J. Booth, and T. Wilson, "Dynamic wave-front generation for the characterization and testing of optical systems," *Opt. Lett.* **23**, 1849–1851 (1998).
- [17] B. R. Boruah, "Dynamic manipulation of a laser beam using a liquid crystal spatial light modulator," *Am. J. Phys.* **77**, 331–336 (2009).
- [18] V. N. Mahajan, "Zernike circle polynomials and optical aberrations of systems with circular pupils," *Appl. Opt.* **33**, 8121–8124 (1994).